Electronic Supplementary Material (ESI) for Soft Matter.

Supporting Information

Unfolding and folding pathway of lysozyme induced by sodium dodecyl sulfate

Yang Sun[a], Pedro L. O. Filho[a], José Junior[b] , Juliana Carvalho[b], Shirley Schreier[b], Cristiano L. P. Oliveira [a,*]

[a] Instituto de Física, Universidade de São Paulo, Rua do Matão 187, São Paulo-SP, 05314-970, Brasil.

[b] Instituto de Quimica, Universidade de São Paulo, Av. Prof. Lineu Prestes 748, São Paulo-SP, 05508-000, Brasil.

* Corresponding author e-mail: crislpo@if.usp.br

EXPERIMENTAL SECTION

Materials

Hen egg white lysozyme (HEWL, CAS Number 12650-88-3) and sodium dodecyl sulfate (SDS) were purchased from Sigma-Aldrich (St. Louis, USA) and were used without further purification. All samples were prepared with 10 mM pH 6.9 PBS buffer (ionic strength 16 mM).

Isothermal titration calorimetry (ITC)

The calorimetric measurements were performed with a MicroCal iTC_{200} (GE Healthcare Life Sciences) placed at the Institute of Physics, University of São Paulo. The sample cell was filled with 200 μL of a solution of 0.03-0.15 mM HEWL, and the titration syringe was filled with 39 μL of 100 mM SDS solution. For each titration step a volume of 1 μL of the concentrated SDS solution was injected into the sample cell. All experiments were done at 25 °C. The obtained heat flux signals (the *fluxogram*) were integrated over time using the Origin™ software supplied by MicroCal™. From this procedure was possible to obtain the molar enthalpies values for each injection (the *enthalpogram*).

Fluorescence measurements

Steady-state fluorescence measurements were carried out using a Cary Eclipse fluorescence spectrophotometer (Varian Ltd.) placed at the Institute of Physics, University of São Paulo. The excitation was set at 290 nm with the emission range between 300–500 nm. Measurements were performed at 25 °C in a 10 mm quartz cuvette (Hellma, Germany) as an average of three accumulations with a scanning speed 200 nm/min, and both of excitation and emission slits widths were 5 nm. Three-dimensional fluorescence spectra were collected with setting excitation from 200 to 350 nm and emission from 300 to 450 nm, and the increment of both excitation and emission are 2.5 nm.

Near- and far-UV circular dichroism (CD) measurements

Far-UV and near-UV circular dichroism (CD) were recorded, respectively, in a 1 cm and 5 cm quartz cuvette on a JASCO J-715 spectropolarimeter (Jasco, Japan) placed at the Institute of Chemistry, University of São Paulo. The experimental data was collected at 25 °C. Wavelength scans were recorded in the range of 195–260 nm (bandwidth 1.0 nm and path 0.1 cm) for far-UV and 250–320 nm (bandwidth 1.0 nm and path 0.5 cm) for near-UV CD. The scanning speed was 20 nm/min and response was 4 seconds with an average of four accumulations. Background contributions from the buffer were subtracted. The results are presented as the mean residue molar ellipticity [θ] (deg cm^2 dmol^{-1}) versus the wavelength (nm). The far-UV CD spectra were analyzed on the program DICHROWEB, which uses SELCON3 algorithms.[1-3]

Small-angle X-ray scattering

Data collection was performed on the laboratory based SAXS equipment Xenocs XEUSS^{TM}, placed at the Institute of Physics, University of São Paulo. The radiation is generated by a GENIX^{TM} source (Cu kα edge, λ=1.54 Å), and the beam focused by a FOX2D^{TM} optics. The beam collimation is performed by two sets of scatterless slits providing a beam spot size of ~1x1 mm at sample position. The 2D data is collected on a Dectris Pilatus^{TM} 300k detector. The samples are placed on reusable quartz capillaries of 1.5 mm in diameter, mounted on stainless steel cases. Therefore the capillaries can be washed and rinsed, permitting the measurements of the sample and buffer at the same conditions. The sample to detector distance was 0.7 m, giving a q range of $0.015<q<0.35$Å^{-1}, where q is the reciprocal space momentum transfer modulus, defined as $q = (4\pi \sin\theta)/\lambda$, where 2θ is the scattering angle and λ is the radiation wavelength. The series of experiments comprised the measurement of the native 150 μM HEWL, 10 mM pure SDS micellar solution, and also samples with HEWL–SDS complexes with different ratios

of SDS. The acquisition time was 1800 s, and temperature was 25 °C. The details of SAXS data analysis and modeling using a model for a core-shell structure with molten globule protein shell were listed below. The model includes molecular constraints and the fits are performed in absolute scale, which increases the reliability of the results[4].

Small-angle X-ray scattering (SAXS) data analysis

The SAXS data was integrated by the use of the program FIT2D.[5] For the integrated 1D data, error estimations, data treatment and normalization in absolute scale was performed by the program SUPERSAXS (Oliveira and Pedersen, unpublished). For absolute scale normalization, the scattering from pure water at 20 °C was used as primary standard.[6] The resulting data, normalized to absolute scale, is displayed as a function of the modulus of the scattering vector q. The SAXS data were firstly analyzed by the IFT method[7] on a slightly different implementation (program WIFT[8]). This method permits the calculation of the pair distance distribution function $p(r)$, which can give a model free indication about the structure in real space.[9, 10] This function is a histogram of all distances between a pair of points within the particles weighted by the excess electron density (which can be both positive and negative) at the points. Structural information derived from the $p(r)$ function can be used for identifying structural features of the system, which can be incorporated into more elaborated models for the micelles and the complexes. This analysis also gives the forward scattering value, $I(0)$, which can be used to estimate the molar mass of the complexes[9]. In some cases, the influence of inter-particle interference effects can be eliminated by omitting a few points at the low-q part of the data.

SAXS data modeling using a core-shell structure with molten globule protein shell

Assuming particles with small aspect ratios, the scattering intensity $I(q)$ that comes from them is given by:[11]

$$I(q) = \left\langle A(q)^2 \right\rangle + \left\langle A(q) \right\rangle^2 [S(q) - 1], \quad (1)$$

where $A(q)$ is the form scattering amplitude of the particles and $S(q)$ is the structure factor. The symbol $\langle\ \rangle$ indicates the average over all possible orientations. For the micelle-protein complexes it was used a decorated micelle model, which uses the assumption that the complexes are core-shell-like particles, with the core formed by the hydrocarbon chains of the surfactant and the shell formed by the polar head of surfactant and protein somehow distributed over the micelle surface.[12] So, for core shell particles, the scattering amplitude is given by:

$$A(q) = \Delta\rho_{shell} \cdot V_{tot} \cdot \phi(qr_{out}) + (\Delta\rho_{core} - \Delta\rho_{shell}) \cdot V_{core} \cdot \phi(qr_{in}) \quad (2)$$

The interfaces were made diffuse by multiplying each term on the Eq. 2 with the factor $e^{-\frac{\sigma^2 q^2}{2}}$, where σ is the width of the Gaussian distribution used to smear the interface. The function $\phi(qr)$ is the normalized scattering amplitude for a sphere, given by:[13]

$$\phi(qr) = 3\frac{\sin(qr) - qr\cos(qr)}{(qr)^3}. \quad (3)$$

Assuming that the complexes have an ellipsoidal shape, the so-called form factor $P(q) = \left\langle A(q)^2 \right\rangle$ is given by:[14]

$$P(q) = \left\langle A(q)^2 \right\rangle = \int_0^{\frac{\pi}{2}} [\Delta\rho_{shell} \cdot V_{tot} \cdot A(qr_{out}) + (\Delta\rho_{core} - \Delta\rho_{shell}) \cdot V_{core} \cdot A(qr_{in})]^2 \sin\alpha d\alpha \quad (4)$$

with $r_{in} = R_{in}(\sin\theta^2 + \varepsilon^2 \cos\theta^2)^{\frac{1}{2}}$ and $r_{out} = R_{out}(\sin\theta^2 + \varepsilon_{out}{}^2 \cos\theta^2)^{\frac{1}{2}}$, where θ is the angle between the scattering vector (of modulus q) and the ellipsoid main axis. The parameters R_{in}, R_{out} and ε are the inner radius, outer radius and aspect ratio of the ellipsoidal object respectively. The outer radius is redefined by $R_{out} = R_{in} + D_{shell}$ and $\varepsilon_{out} = \frac{\varepsilon R_{in} + D_{shell}}{R_{in} + D_{shell}}$, where D_{shell} is the

thickness of the shell. The use of a different aspect ratio factors factor for the shell is made to keep the shell thickness constant. $\Delta\rho_{shell}$ and $\Delta\rho_{core}$ are the excess scattering length density of the shell (made by the heads/polar groups of the surfactants and protein) and core (made by the tails/hydrocarbon chains) of the ellipsoidal complex respectively. The parameters V_{core} and V_{tot} correspond to the volume of the core and total volume (i.e., $V_{core} + V_{shell}$).

In some cases it was necessary to include a structure factor for the aggregation of the core-shell structures. Several possibilities were tried but the data was reasonably described by a simple globular aggregate with an overall Radius of Gyration R_G:[15]

$$S(q) = 1 + S_{C2} \exp\left(-q^2 R_G^2 / 3\right), \quad (5)$$

where S_{C2} is the scale factor of the aggregate, which is related to the fraction of aggregated core-shell structures and R_G is the average radius of Gyration of the aggregate.

Since the fittings were done in absolute scale of intensity, this allow us to impose several molecular constraints and also take into account available information that comes from the molecules in the system [4].

Knowing the number of electrons per tail and head of the SDS molecules ($N_{el(T)} = 97e$ and $N_{el(H)} = 59e$) as well as the volume of tail and head ($V_T = 355.1\text{Å}^3$ and $V_H = 60.53\text{Å}^3$ [4]) one is able to evaluate the electron density of tail and head as

$$\rho_T = \frac{N_{el(T)}}{V_T}, \quad (6)$$

$$\rho_H = \frac{N_{el(H)}}{V_H}. \quad (7)$$

Taking the electron density of water ($\rho_{WT} = 0.3334 \frac{e}{\text{Å}}$) as a reference, one can write the excess

electron density for the tail and head:

$$\Delta\rho_T = \rho_T - \rho_{wt}, \tag{8}$$

$$\Delta\rho_H = \rho_H - \rho_{wt}. \tag{9}$$

The volume of the core (in Å^3) will be

$$V_{core} = \frac{4}{3}\pi\varepsilon R_{in}{}^3. \tag{10}$$

The aggregation number will be

$$N_{Agg} = \frac{V_{core}}{V_T}. \tag{11}$$

The concentration of surfactant that forms micelles (mM) is given by:

$$C = c - c_{free}, \tag{12}$$

while the number of surfactant molecules that forms micelles (molecules/cm^3):

$$N = (c - c_{free}) \cdot 10^{-6} \cdot N_A, \tag{13}$$

where "N_A" is the Avogadro number (6.02×10^{23}). So, the number of micelles (micelles/cm^3):

$$n_{mic} = \frac{N}{N_{agg}}. \tag{14}$$

If one assumes that all the protein in the system forms a complex with the micelles, the mass of protein per micelle (g/micelle) will be

$$m_{prot} = \frac{c_{prot} \cdot 10^3}{n_{mic}}. \tag{15}$$

For protein, the average excess contrast scattering length per mass of protein is $\Delta\rho_m = 2.0\times10^{10}\ \frac{cm}{g}$.[6] Dividing it by the classical electron radius (Thomson radius),

$r_T = 2.82 \times 10^{-13} cm$, we will have $\frac{\Delta\rho_m}{r_T}$, i.e., the amount of electrons per mass of protein (in electrons/g). Then, the excess of electrons in each micelle due to the protein will be (in electrons/micelle):

$$N_{el(prot)} = \frac{\Delta\rho_m}{r_T} m_{prot} . \qquad (16)$$

If one assumes that the proteins stays at the shell of the complex micelle-protein we will have a total number of electrons of

$$N_{el(shell)} = N_{agg} V_H \Delta\rho_H + N_{el(prot)} . \qquad (17)$$

The total volume will be

$$V_{tot} = \frac{4}{3} \pi \varepsilon_{out} R_{out}^{\ 3} . \qquad (18)$$

Then, the volume of the shell will be

$$V_{shell} = V_{tot} - V_{core} . \qquad (19)$$

A useful parameter is the water fraction in the shell, calculated by

$$x_{wt} = \frac{V_{shell} - N_{agg} V_H - m_{prot} \bar{v}}{V_{shell}} , \qquad (20)$$

where $\bar{v}$ is the specific volume of a protein, which is in general $0.72 \frac{cm^3}{g}$. The excess of contrast of scattering length, for shell and core, will be:

$$\Delta\rho_{shell} = Sc_{shell} \frac{N_{el(shell)} \cdot r_T}{V_{shell}} , \qquad (21)$$

$$\Delta\rho_{core} = \Delta\rho_T \cdot r_T , \qquad (22)$$

where Sc_{shell} is a scale factor which corrects some possible differences between the theoretical $\Delta\rho_{shell}$ and the real one on the system. This can be an indication of small changes in the

hydration of the groups on the shell.

The final expression for the modeled intensity is:

$$I(q) = Sc \cdot n_{mic} \cdot [P(q) + \langle A(q) \rangle^2 (S(q) - 1)] + back \quad (23)$$

The parameter Sc is an overall scale factor, which can correct for small variations on the surfactant concentration. In almost all cases presented in this work, its value was always 1.

The parameters of electron density of the solvent (electrons/Å^3), ρ_{WT}; Volume of the surfactant tail group (Å^3), V_T; Volume of the surfactant head group (Å^3), V_H; Number of electrons of the tail, $N_{el(T)}$; Number of electrons of the head, $N_{el(H)}$;Total concentration of surfactant (mM), c; Concentration of surfactant that does not form micelles (mM), c_{free} and concentration of protein (mg/mL), c_{prot}, where all fixed. The remaining variables were optimized against the experimental data. The aggregation number and the mass or protein per micelle are calculated from the modeling results. All data were fit on absolute scale, including the protein and surfactant concentration and the proper scattering length densities, which significantly constrain the model.

Results

The aggregation and dissolution of system in different ratios of SDS/HEWL

HEWL is a small globular enzyme with 18 cationic and 12 anionic residues. The isoelectric point is at pH 11, and the positive net charge is 8 in an aqueous solution with a pH of 6.5.[16] The interactions of HEWL with oppositely charged surfactants such as SDS, are made on several different associating features.[17] First, the oppositely charged macromolecules are known to form a precipitate.[18] Second, this precipitate can be resolubilized by adding more surfactant.[19] The soluble complexes are reported to be of two types, of different size.[18] Third, the resolubilization process is by phase behavioral studies shown to proceed via a narrow region of a gel.[20] As see from Fig. S1, there is a precipitation in the low ratio of SDS/HEWL, and then, the precipitate is resolubilized with addition of more SDS molecules.

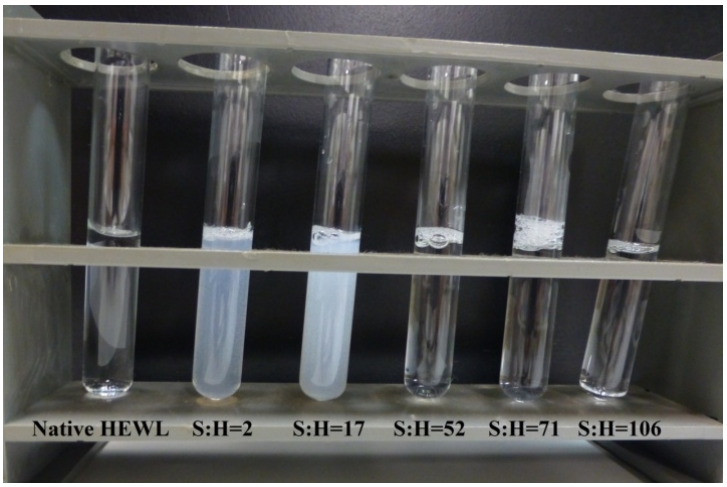

Figure S1. The photograph of HEWL in the presence different ratios of SDS (presented as S:H), [HEWL]=0.15 mM.

Three dimensional fluorescence spectra

The fluorescence inner filter effect is corrected by the Eq. 24 for Peak *b* with the excitation of 270 nm.[21, 22]

$$\frac{I^{\text{corr}}}{I^{\text{obsd}}} = 10^{0.5A_{\text{x}}+0.5A_{\text{m}}} \tag{24}$$

Table S1 Three-dimensional fluorescence spectral parameters of native HEWL (0.06 mM) with different ratios of SDS (presented as S:H)

Selected points (ratio of SDS/HEWL)	Peak *a* (excitation/emission, nm/nm), intensity (a.u.)	Peak *b* (excitation/emission, nm/nm), intensity (a.u.)
Native HEWL	290/347, 267.2	275/344, 252.2
T1 (S:H=8)	290/347, 193.1	275/343, 200.4
T2 (S:H=28.1)	290/346, 186.3	–
T3 (S:H=42.0)	290/344, 140.2	–
T4 (S:H=55.1)	290/342, 120.4	–
T5 (S:H=73.3)	290/340, 90.8	–
T6 (S:H=85.1)	290/338, 86	–
T7 (S:H=104)	290/340, 91.4	–
T8 (S:H=113)	290/340, 100.6	–
T9 (S:H=123)	290/341, 153.7	270/340, 160.6
T10 (S:H=143)	290/342, 194.6	270/340, 200.7
T11 (S:H=167)	290/343, 202.2	270/340, 232.3

Absorption spectra

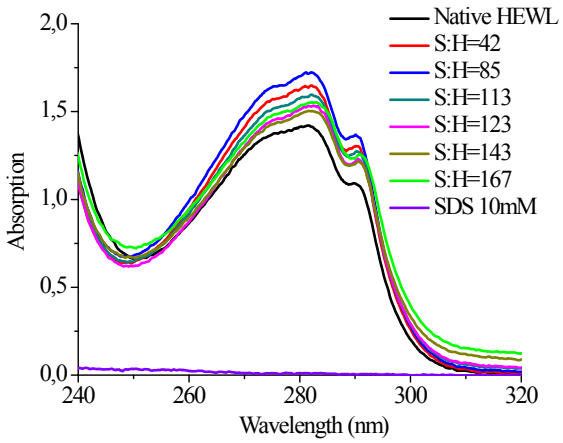

Figure S2. Absorption spectroscopy of native HEWL with different ratio of SDS, and the concentrations of HEWL and SDS are the same as the fluorescence measurement.

The details of CD spectra of HEWL with different SDS/HEWL ratios

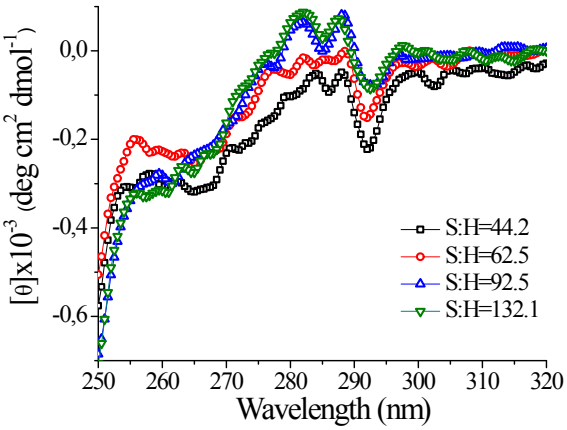

Figure S3. Near-UV CD spectra of complex with different ratios of SDS/HEWL (presented as S:H).

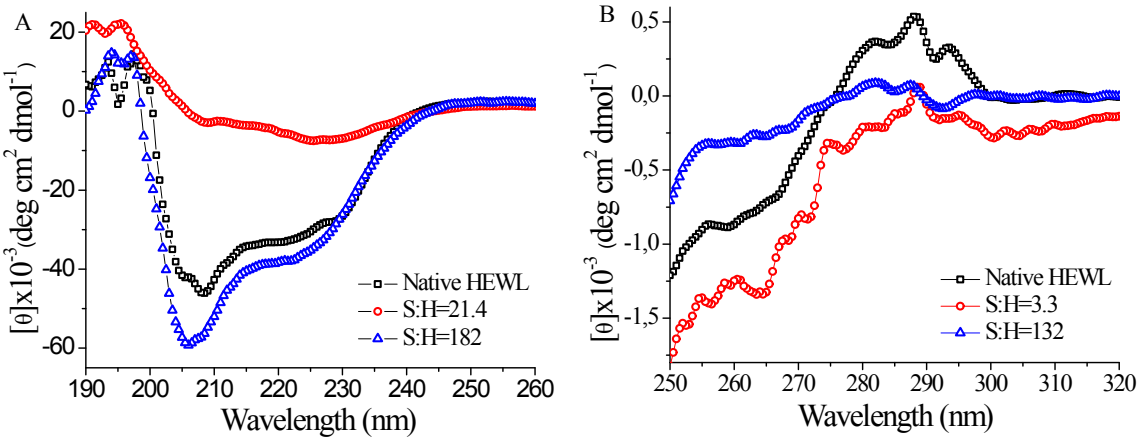

Figure S4. Far-UV CD (A) and near-UV CD (B) spectra of native HEWL with different ratios of SDS (presented as S:H).

Comparison of theoretical scattering intensity of HEWL with experimental SAXS data

Since the atomic resolution structure of HEWL is known, one can compare the theoretical scattering intensity calculated from the atomic coordinates with the experimental data, which was performed by using of the program CRYSOL.[23] As shown in Fig. S5, the experimental SAXS data of HEWL and complex with ratio of SDS/HEWL 2 are very well described by the theoretical intensity calculated by the atomic coordinates of HEWL (6LYZ.PBD). This indicates that the particles on these two samples have similar shape as in the crystal structure, while the shape of particles on samples with higher ratio becomes more and more different than the native HEWL structure.

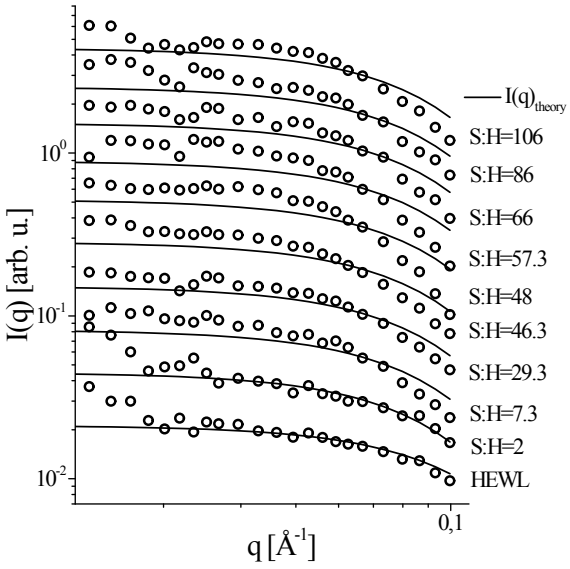

Figure S5. Fitting with the theoretical intensity of atomic-resolution crystal structure of HEWL (PDB: 6LYZ, line). The experimental data are shown as open circles, and the theoretical fits are shown as continuous lines. [HEWL] = 0.15 mM, around 2.2 mg/mL, [SDS] = 0.9-16 mM. The different ratio of SDS/HEWL is presented as S:H.

The SAXS data associated IFT results and decorated model for native HEWL, "*aggregate **1***" *and* "*aggregate **2***"

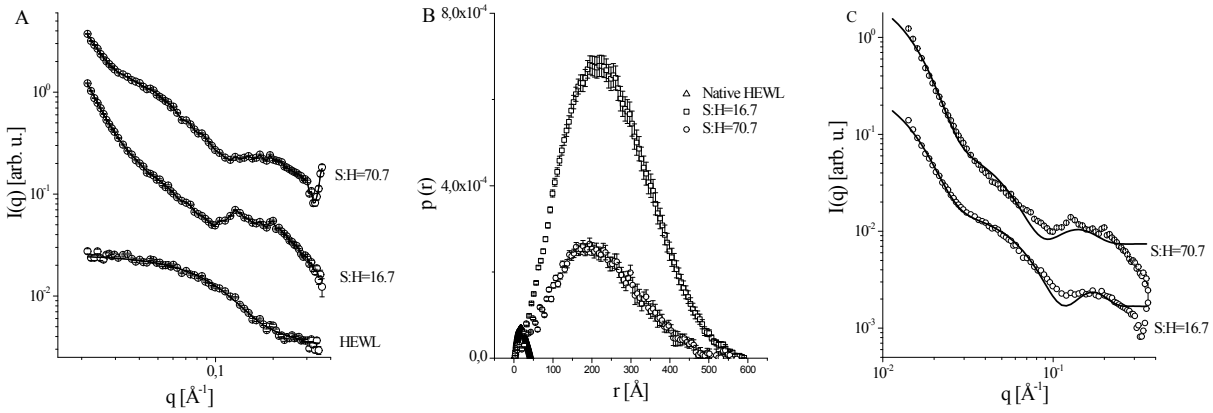

Figure S6 (A): The SAXS results and associated IFT results for native HEWL, and the ratio of SDS/HEWL 16.7 and 70.7 (presented as S:H). (B): The corresponding pair distance distribution function $p(r)$. (C): Model fits the data of with the ratio of SDS/HEWL 16.7 and 70.7, respectively.

The Dynamic Light Scattering (DLS) details of "*aggregate **1***" *and* "*aggregate **2***"

The phase behavior for the HEWL−SDS−water system in the range of 80−100 wt % water has been fully described by Morén et al.[20, 24, 25] Three different phases are obtained within these concentration limits. First, a precipitate of the net-neutralized macromolecule is formed (S), the more SDS adding leads to complexes with a net-negative charge, which due to the dissolution of precipitate. For concentrations just above the CAC (critical aggregation concentration) the repulsion caused by the negative charge is not large enough to overcome the hydrophobic attraction between the complexes, which leads to the gel formation, and a sketch of the structure of the aggregate.[17, 24] For higher concentration of lysoyzme, the system is dominated by repulsion and soluble protein−surfactant complexes form a clear nonviscous solution phase, in which, there is two-phase system containing dispersions of a gel. The solution phase is of low viscosity containing finite aggregates where the protein is solubilized by micelle-like aggregates.[26]

The complex sizes of HEWL/SDS were also measured using Dynamic Light Scattering (BIC Particle Sizing Software 90 Plus, Brookhaven Instruments Corp.) at the Institute of Physics, University of São Paulo, in order to investigate the aggregation behavior in the different concentration of HEWL. As seen from Fig. S7A, for high concentration of HEWL (0.15 mM), the aggregates occurs in both of low and high ratio of SDS (SDS/HEWL, presented as S:H = 17 and 71). While, for low concentration of HEWL (Fig. S7B, 0.06 mM), one can clearly see that there is aggregation in the low ratio of SDS (S:H=28, aggregates **1**) and also for a high ratio of SDS (S:H=85, aggregates **2**), but the aggregates at high ratio of SDS are much less visible in HEWL (0.06 mM) then for HEWL (0.15 mM). This indicates that the concentration of aggregated fraction is very small for low protein concentration,[17] which makes difficult to be detected by spectral techniques (fluorescence or CD) due to the low concentration of protein used in experiment (0.06 mM for fluorescence and 0.03 mM for CD). These results are accordance with that of Morén et al, which demonstrates that the solution phase is of low viscosity containing finite aggregates where the protein is solubilized by micelle-like aggregates in the higher weight phase region of lysoyzme.[24, 26]

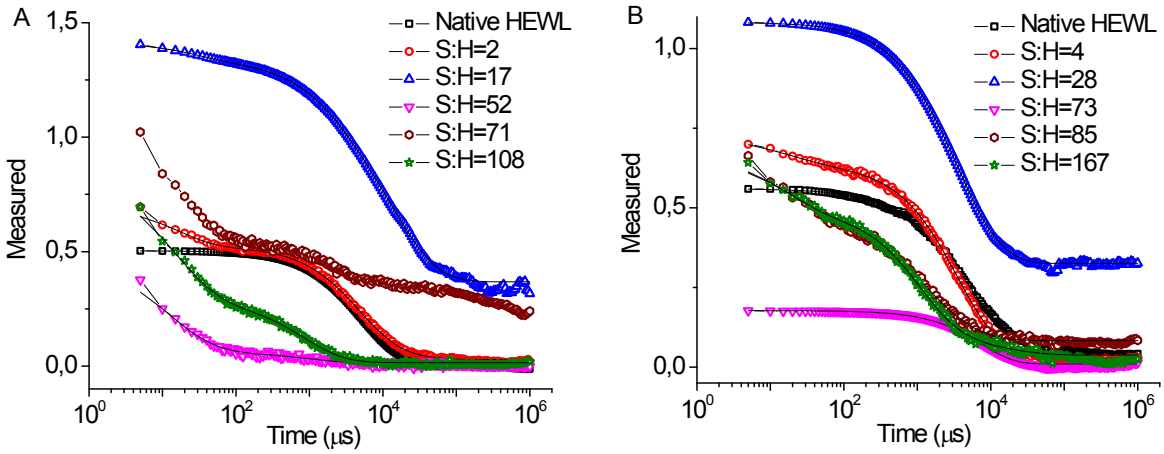

Figure S7. The complex sizes of HEWL/SDS were measured using dynamic light scattering (BIC Particle Sizing Software 90 Plus, Brookhaven Instruments Corp.). A: the correlation curves of 0.15 mM HEWL in the presence of different ratio of SDS (presented as S:H); B: the correlation curves of 0.06 mM HEWL in the presence of different ratio of SDS (presented as S:H).

Conductometric measurement

The conductivity of the varying concentrations of SDS solutions was measured with a QUIMIS Q795M2 conductometer (QUIMIS, Brazil) at the Institute of Physics, University of São Paulo. The measurement was performed at 20 °C, which is controlled by a water-circulating bath. Fig.S8 presents the experimental data of conductivity vs different SDS concentration, and its corresponding first derivative. The CMC was obtained by a method proposed by Carpena et al.[27] This method is based on the fit of the experimental raw data to a simple nonlinear function obtained by direct integration of a Boltzmann type sigmoid function. In this case, CMC is 4.1 ± 0.1 mM.

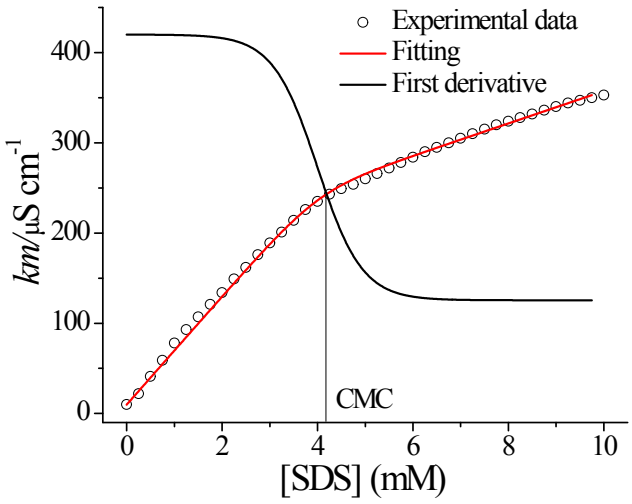

Figure S8. The conductivity, k in μS cm^{-1}, of different SDS concentration in PBS, pH 6.9, ionic strength is 16 mM, T = 20 ºC.

Unfolding and folding of HEWL induced by SDS in different binding stages

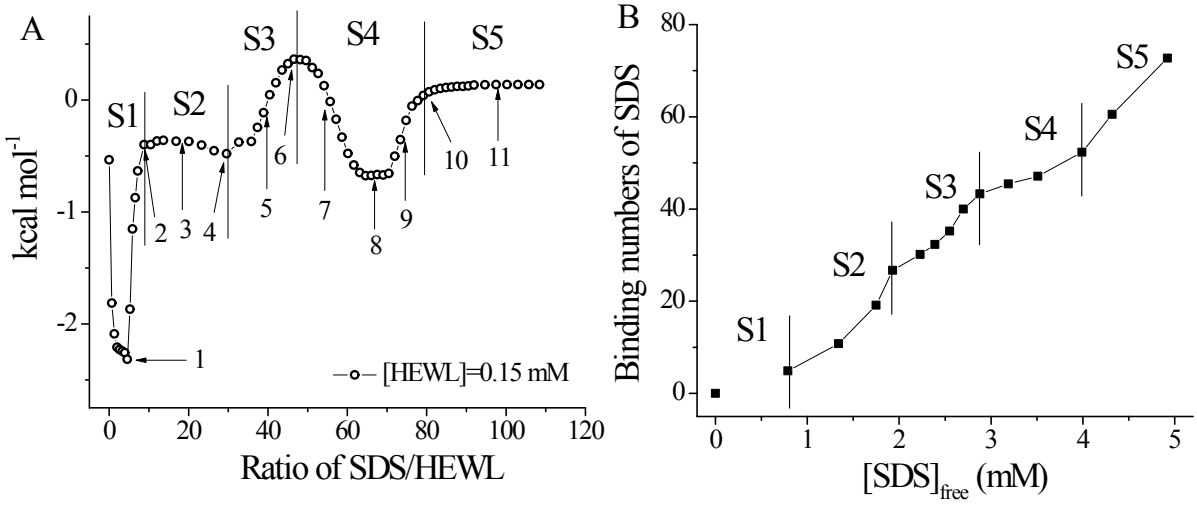

Figure S9. (A): ITC enthalpogram for the titration of SDS (100 mM) into 0.15 mM HEWL, and the abscissa is presented as ratio of SDS/HEWL. (B): Free SDS concentration plotted vs. the binding number of SDS molecules. This plot corresponds to characteristic multistep Jones's and Tanford's classical SDS binding isotherm.[28, 29] S1: monomeric binding of SDS molecules; S2: dissolution of precipitation; S3: unfolding of HEWL by cooperative binding of electrostatic and hydrophobic interaction of SDS; S4: stripping of HEWL from complexes and recasting the decorated micelles; S5: bulk free micelles of SDS binding. The initial strong binding at low SDS is followed by a slow-rising part of the binding isothermal for intermediate concentrations. Later, pure SDS micelles form for free SDS concentration beyond the CMC (4.1±0.1 mM obtained from the conductivity, Fig. S8).

References

1. L. Whitmore and B. A. Wallace, *Nucleic Acids Research*, 2004, **32**, W668-W673.
2. L. Whitmore and B. A. Wallace, *Biopolymers*, 2008, **89**, 392-400.
3. A. Lobley, L. Whitmore and B. A. Wallace, *Bioinformatics*, 2002, **18**, 211-212.
4. L. Giehm, C. Oliveira, G. Christiansen, J. Pedersen and D. Otzen, *Journal of Molecular Biology*, 2010, **401**, 115-133.
5. A. P. Hammersley, S. O. Svensson, M. Hanfland, A. N. Fitch and D. Hausermann, *High Pressure Research*, 1996, **14**, 235-248.
6. S. Manet, A. Lecchi, M. Imperor-Clerc, V. Zholobenko, D. Durand, C. L. P. Oliveira, J. S. Pedersen, I. Grillo, F. Meneau and C. Rochas, *Journal of Physical Chemistry B*, 2011, **115**, 11318-11329.
7. O. Glatter, *Journal of Applied Crystallography*, 1977, **10**, 415-421.
8. C. L. P. Oliveira, M. A. Behrens, J. S. Pedersen, K. Erlacher, D. Otzen and J. S. Pedersen, *Journal of Molecular Biology*, 2009, **387**, 147-161.
9. C. L. P. Oliveira, in *Current Trends in X-Ray Crystallography*, ed. D. A. Chandrasekaran, InTech, 2011, ch. 16, pp. 367-392.
10. C. Alves, J. S. Pedersen and C. L. Pinto Oliveira, *Journal of Applied Crystallography*, 2014, **47**, 84-94.
11. J. S. Pedersen, *Advances in Colloid and Interface Science*, 1997, **70**.
12. N. Lorenzen, S. B. Nielsen, A. K. Buell, J. D. Kaspersen, P. Arosio, B. S. Vad, W. Paslawski, G. Christiansen, Z. Valnickova-Hansen, M. Andreasen, J. J. Enghild, J. S. Pedersen, C. M. Dobson, T. P. J. Knowles and D. E. Otzen, *Journal of the American Chemical Society*, 2014, **136**, 3859-3868.
13. L. Rayleigh, *Proceedings of the Royal Society of London Series a-Containing Papers of a Mathematical and Physical Character*, 1910, **84**.
14. F. J. Rogers and D. A. Young, *Physical Review A*, 1984, **30**.
15. C. L. P. Oliveira, A. M. Monteiro and A. M. Figueiredo Neto, *Brazilian Journal of Physics*, 2014, **44**, 753–764.
16. C. Tanford and M. L. Wagner, *Journal of the American Chemical Society*, 1954, **76**, 3331-3336.
17. A. Stenstam, A. Khan and H. Wennerstrom, *Langmuir*, 2001, **17**, 7513-7520.
18. A. Valstar, W. Brown and M. Almgren, *Langmuir*, 1999, **15**, 2366-2374.
19. K. Fukushima, Y. Murata, N. Nishikido, G. Sugihara and M. Tanaka, *Bulletin of the Chemical Society of Japan*, 1981, **54**, 3122-3127.
20. A. K. Moren and A. Khan, *Langmuir*, 1995, **11**, 3636-3643.
21. C. B. Nettles, II, J. Hu and D. Zhang, *Analytical Chemistry*, 2015, **87**, 4917-4924.
22. A. V. Fonin, A. I. Sulatskaya, I. M. Kuznetsova and K. K. Turoverov, *Plos One*, 2014, **9**.
23. D. Svergun, C. Barberato and M. H. J. Koch, *Journal of Applied Crystallography*, 1995, **28**, 768-773.
24. A. Stenstam, G. Montalvo, I. Grillo and M. Gradzielski, *Journal of Physical Chemistry B*, 2003, **107**, 12331-12338.
25. A. K. Moren and A. Khan, *Langmuir*, 1998, **14**, 6818-6826.
26. A. K. Moren, M. Nyden, O. Soderman and A. Khan, *Langmuir*, 1999, **15**, 5480-5488.
27. P. Carpena, J. Aguiar, P. Bernaola-Galvan and C. C. Ruiz, *Langmuir*, 2002, **18**, 6054-6058.
28. J. A. Reynolds and C. Tanford, *Journal of Biological Chemistry*, 1970, **245**, 5161-&.
29. M. N. Jones, *Chemical Society Reviews*, 1992, **21**, 127-136.